

α -Amanitin Blocks Translocation by Human RNA Polymerase II*

Received for publication, February 26, 2004
Published, JBC Papers in Press, April 19, 2004, DOI 10.1074/jbc.M402163200

Xue Q. Gong[‡], Yuri A. Nediaikov, and Zachary F. Burton[§]

From the Department of Biochemistry and Molecular Biology, Michigan State University, East Lansing, Michigan 48824-1319

Our laboratory has developed methods for transient state kinetic analysis of human RNA polymerase II elongation. In these studies, multiple conformations of the RNA polymerase II elongation complex were revealed by their distinct elongation potential and differing dependence on nucleoside triphosphate substrate. Among these are conformations that appear to correspond to different translocation states of the DNA template and RNA-DNA hybrid. Using α -amanitin as a dynamic probe of the RNA polymerase II mechanism, we show that the most highly poised conformation of the elongation complex, which we interpreted previously as the posttranslocated state, is selectively resistant to inhibition with α -amanitin. Because initially resistant elongation complexes form only a single phosphodiester bond before being rendered inactive in the following bond addition cycle, α -amanitin inhibits elongation at each translocation step.

“Among those foods that are eaten carelessly, I would place mushrooms. Although mushrooms taste wonderful, they have fallen into disrepute because of a shocking murder. They were the means by which the emperor Tiberius Claudius was poisoned by his wife Agrippina. Thus, she gave the world a poison worse still—her own son Nero” (translation from Latin, Pliny the Elder). The poisoning occurred in the year 54 A.D. Ingestion of the death cap mushroom *Amanita phalloides* kills humans by destroying the liver and damaging the kidneys (1, 2). For an adult, a lethal dose may be as little as 3 g of the more than ample mushroom cap (6–16 cm diameter), and symptoms do not develop until 8–24 h after ingestion. Victims report that the taste of the deadly mushroom does not presage the agony to come. Severe cases require liver and kidney transplant, treatments unavailable to the unfortunate Claudius. The molecular target of α -amanitin is RNAP¹ II, for which the toxin is a potent and specific inhibitor (3).

After three decades of study, however, the mode of toxin action has not been resolved. Recently, an x-ray structure was published of α -amanitin soaked into crystals of yeast RNAP II, indicating many of the key atomic contacts that contribute to RNAP II inactivation (4). Multiple strong interactions between

α -amanitin and RNAP II are found in the “funnel,” the “cleft,” and the key “bridge α -helix” regions of the Rpb1 subunit, which constitute the RNAP II “secondary pore” or “pore 1,” a solvent-accessible channel into the RNAP II active site. Contacts to the bridge helix are on the opposite face from the RNAP II active site, indicating that α -amanitin is unlikely to block catalysis directly. Bound α -amanitin partially occludes the pore, which has been presumed to be a channel for NTP substrate loading (4–6) but may be primarily the route of pyrophosphate release (7). Contacts of α -amanitin to the bridge helix are intriguing because bending of the bridge α -helix is thought to drive translocation of the RNA-DNA hybrid (6–9). Translocation is essential during each bond addition cycle to move the RNA-DNA hybrid away from the space that must be cleared to load the next substrate NTP into the active site. Because α -amanitin binds to RNAP II with a relatively straight conformation of the bridge helix and because of key contacts between the bridge helix and α -amanitin, Kornberg and co-workers (4) suggested that α -amanitin may block translocation by blocking bridge helix bending. Several reports in the literature, however, indicate that RNAP II may be capable of forming multiple phosphodiester bonds without dissociation of α -amanitin (10, 11), so α -amanitin must allow occasional translocation without dissociation from RNAP II.

Recently, we developed a method for transient state kinetic analysis of RNAP II elongation stimulated by transcription factor IIF (TFIIF) and hepatitis δ antigen (HDAG) (7). After stalling RNAP II briefly by withholding the next substrate NTP, we demonstrated that the EC fractionated into multiple conformational states with distinct elongation kinetics. We and others showed that RNAP II utilizes a branched kinetic mechanism in which the EC partitions between an active synthesis mode and a pausing mode (12–15). The forward synthesis pathway is intricate, involving NTP substrate-induced fit and multiple conformational states, interpreted as distinct translocation states. Notably, our studies strongly suggest that the incoming substrate NTP first pairs with its cognate DNA template base and then induces translocation of the RNA-DNA hybrid, clearing space to seat the incoming dNMP-NTP base pair in the RNAP II active site for chemistry (7).

HDAG is a viral RNAP II elongation factor encoded by hepatitis δ virus (HDV) (16, 17). HDV has an unusual covalently closed circular RNA genome of about 1.7 kilobases in length, which forms a compact, mostly double-stranded RNA rod structure. The HDV rod is maintained and transported as a satellite particle of hepatitis B virus (HBV), and co-infection with HDV and HBV is associated with severe and chronic presentations of human HBV infection. For the purposes of this paper, HDAG was used to facilitate the kinetic analysis of RNAP II elongation so that α -amanitin inhibition could be analyzed more easily (7, 15, 18).

In this work we present the first study in which α -amanitin is added to RNAP II ECs engaged in active RNA synthesis. We employ a “running start” assay in which a large fraction of

* This work was supported by Grant GM57461 from the National Institutes of Health (to Z. F. B.). The costs of publication of this article were defrayed in part by the payment of page charges. This article must therefore be hereby marked “advertisement” in accordance with 18 U.S.C. Section 1734 solely to indicate this fact.

[‡] Supported by the Michigan State University Development Foundation Initiative in Gene Expression in Development and Disease.

[§] Recipient of support from the Michigan State University Agricultural Experiment Station. To whom correspondence should be addressed. Tel.: 517-353-0859; Fax: 517-353-9334; E-mail: burton@msu.edu.

¹ The abbreviations used are: RNAP, RNA polymerase; TF, transcription factor; HDAG, hepatitis δ antigen; EC, elongation complex; HDV, hepatitis δ virus; HBV, hepatitis B virus; C40, 40-nucleotide RNA ending in a 3'-CMP.

RNAP II ECs are committed to the active elongation pathway at the time of inhibitor addition (7, 15, 19). Because we utilize rapid quench technology, we can monitor inhibition and elongation with millisecond time resolution, improving the quality of the analysis. Strikingly, we find that the most highly poised conformation of RNAP II ECs is selectively resistant to α -amanitin inhibition. Previously, we identified the most highly poised EC as being posttranslocated, and studies with α -amanitin inhibition appear to confirm this identification. These highly poised ECs are capable of binding NTP substrate and adding a single phosphodiester bond, but they become highly sensitive to α -amanitin inhibition in the subsequent bond addition cycle, indicating that they become incapable of progressing through the next translocation step.

EXPERIMENTAL PROCEDURES

Cell Culture, Extracts, and Proteins—HeLa cells were purchased from the National Cell Culture Center (Minneapolis, MN). Extracts of HeLa cell nuclei were prepared as described previously (20). Recombinant HDAG was purified as described by Yamaguchi *et al.* (18).

Preparation of Elongation Complexes—Detailed protocols for rapid quench-flow experiments have been published previously (7, 15, 19, 21). Briefly, 32 P-labeled C40 (40-nucleotide RNA ending in a 3'-CMP) RNAP II ECs were formed on MagneSphere (Promega, Madison, WI) metal bead-immobilized templates. Initiation was from the adenovirus major late promoter, which was amplified by polymerase chain reaction using a 5'-biotinylated upstream primer. Biotinylation allowed immobilization on streptavidin-coated beads. Transcription factors were derived from an extract of HeLa nuclei. Initiation and elongation were in transcription buffer (12 mM HEPES, pH 7.9, 12% v/v glycerol, 60 mM KCl (unless otherwise specified), 0.12 mM EDTA, 0.12 mM EGTA, 1.2 mM dithiothreitol, and 0.003% IGEPAL CA-630 (Sigma)) containing 8 mM MgCl₂. All steps were at 25 °C. The adenovirus major late promoter template has a modified downstream sequence (ACTCTCTCCCCTTCTCTTTCCTTCTCTTCCCTCTCTCC⁴⁰AAAGGCCTTT⁵⁰). The purpose of the 39-nucleotide CT-cassette is to synthesize C40 with addition of 300 μ M adenylyl(3'→5')cytidine dinucleotide, 10 μ M dATP, 5 μ Ci of [α - 32 P]CTP/reaction (800 Ci/mmol), and 20 μ M UTP, bypassing the requirement for addition of ATP and GTP. C40 ECs are washed with 1% Sarkosyl and 0.5 M KCl buffer to dissociate initiation, elongation, pausing, and termination factors contributed by the HeLa extract and then are re-equilibrated with transcription buffer containing 8 mM MgCl₂ and 20 μ M CTP and UTP. A functionally saturating concentration of HDAG (77 pmol/reaction) is then added. Subsequent steps are performed using the Kintek rapid chemical quench-flow (RQF-3) instrument (Kintek Corporation, Austin, TX), which allows reactions to be started and stopped with millisecond precision.

Running Start Protocol—The running start protocol has been described previously (7, 15, 19, 21). Elongation was through the sequence ⁴⁰CAAAGGCC⁴⁷. C40 ECs were advanced to A43 by bench top addition of 100 μ M (working concentration) ATP for 60 s. The reaction shown in Fig. 1 was done with the Kintek RQF-3 run in pulse-chase mode. A43 ECs were loaded through the left sample port. α -Amanitin (Sigma) was added through the right sample port. 1 mM GTP (working concentration) was added through the quench syringe. The reaction was stopped in the collection tube, which contained 300 μ l of 0.5 M EDTA. To analyze the data shown in Fig. 1C, all inhibition curves were adjusted to begin at 50% total ECs so that data from different experiments could be compared more easily. For the experiments shown in Fig. 2, the RQF-3 was operated in the standard mode. A43 ECs were loaded through the left sample port. GTP and α -amanitin were combined and loaded through the right sample port. 0.5 M EDTA was added through the quench syringe. ECs were collected with a magnetic particle separator and processed by electrophoresis. Gel bands were quantitated using an Amersham Biosciences PhosphorImager.

RESULTS AND DISCUSSION

RNAP II transcriptional stalling was induced by withholding the next substrate NTP. Upon stalling, the EC was observed to fractionate between multiple functional states. In kinetic analyses, these states were identified as populations of ECs with different rates of elongation and different responses to NTP substrate. Conformational states were shown not to be an artifact of RNAP II purification but rather to reflect distinct

conformations of a dynamic enzyme as it progresses between alternate functional modes (7, 15). One proof of this point was that different collections of elongation factors reallocated the distribution of RNAP II ECs, so treatments after purification determined EC elongation potential.

Because the RNAP II EC fractionates into multiple conformational states at a stall point, we reasoned that these states might have different sensitivities to and/or binding affinities for α -amanitin. We therefore developed a reaction protocol in which α -amanitin was added to the stalled EC either at the same time or just before substrate NTPs (Fig. 1). The purpose of this experimental design was to determine the kinetics for establishing inhibition at different α -amanitin concentrations. 32 P-Labeled C40 RNAP II ECs were purified on bead-immobilized templates by Sarkosyl and salt washing. To facilitate elongation, a functionally saturating amount of the RNAP II elongation factor HDAG was added. C40 ECs were then advanced to and stalled at A43 for 60 s by addition of 100 μ M ATP. During the stall, samples were injected into the rapid quench-flow apparatus. Rapid mixing combined α -amanitin with ECs, and after a variable incubation, reactions were chased for 0.145 s with 1 mM GTP (0.145 s is sufficient for all ECs on the active elongation pathway to complete the G44 bond). ECs that failed to bind α -amanitin or remained active despite binding toxin were extended to G44 or longer products.

This experiment supports the existence of three distinct conformations of the RNAP II EC at the A43 stall position (here designated A43a, A43b, and A43c; Fig. 1C) based on their differential sensitivity to α -amanitin. The A43a phase is the most highly sensitive to inhibition. A43a represents about 5% of total ECs and is most easily observed at 1 and 2 μ M α -amanitin. The A43b phase EC appears to represent about 30% of total ECs. For the A43b phase, the rate of inhibition increases as the α -amanitin concentration increases (Fig. 1, C and D), showing that the inhibition of A43b ECs is limited by the rate of α -amanitin binding. By contrast, A43c ECs are highly resistant to α -amanitin inhibition, and the rate of their inactivation does not increase between 10 and 50 μ M α -amanitin concentration, indicating that an EC conformational change (A43c → A43b) is required for their inhibition. The A43c EC is highly resistant to α -amanitin binding and/or inactivation for G44 synthesis but becomes highly sensitive to inhibition in the subsequent bond transition from G44 → G45.

α -Amanitin Fails to Inhibit the Posttranslocated RNAP II EC—To characterize the α -amanitin-resistant A43c EC, we did the experiments shown in Fig. 2, in which increasing α -amanitin concentrations were combined with stalled A43 ECs at the same time as GTP substrate addition. Inhibition of G44 synthesis was observed at both high (500 μ M) and low (5 μ M) GTP concentrations, and multiple α -amanitin concentrations were tested from 10 μ M to 1 mM. Rates of G44 synthesis were tracked for up to 1 s. As shown previously, in the absence of α -amanitin, rate curves are notably biphasic up to 0.1 s, with a rapid burst phase (A43c) and a slower phase (here designated A43a + A43b) (7, 15). Using the experimental format of Fig. 2, the A43a and A43b conformational states of the RNAP II EC cannot be distinguished as they were in the experiments shown in Fig. 1. As expected, the amplitudes of the A43c and A43a + A43b phases are dependent on the GTP substrate concentration. Previously, the more highly poised A43c phase was interpreted as being posttranslocated, and the less highly poised and more GTP-dependent A43a + A43b phase was interpreted as being pretranslocated (7). We show here that the highly poised A43c reaction phase is resistant to 1 mM α -amanitin, but the A43a + A43b phase is fully sensitive. Because the highly poised A43c phase of the reaction resists 1 mM α -amanitin even at 5 μ M GTP

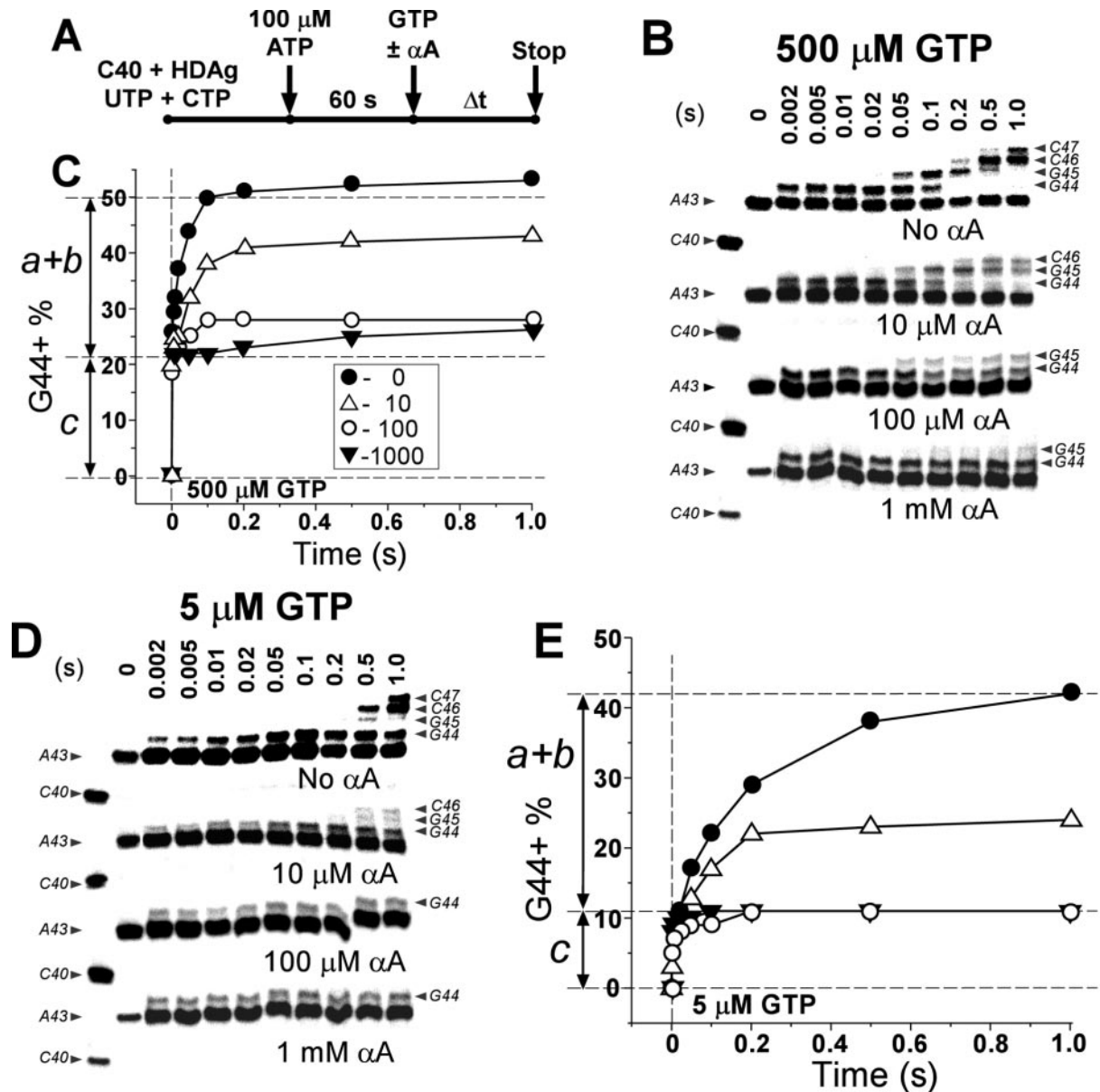


FIG. 2. The A43c (posttranslocated) reaction phase is highly resistant to α -amanitin inhibition. *A*, reaction protocol. α A, α -amanitin. *B* and *C*, kinetics of RNAP II elongation in the presence of 500 μ M GTP. *B*, gel data. *C*, PhosphorImager quantitation. *D* and *E*, kinetics of RNAP II elongation in the presence of 5 μ M GTP. *D*, gel data. *E*, PhosphorImager quantitation. G44+ % indicates the percent of total ECs extended to G44 or longer positions. α -Amanitin concentrations are given in μ M units in *C* and *E* according to the key in *C*.

step inhibited, A43a, A43b, and A43c would all be expected to advance to G44 before being inhibited. The 60-s delay at A43 is considered sufficient for all stalled ECs to dissociate pyrophosphate (7).

We proposed previously the NTP-driven translocation model to describe the RNAP II elongation mechanism (7). One of the major observations on which our model relied was that at a transcriptional stall point, the EC fractionated into multiple conformations, interpreted as distinct translocation states. Using α -amanitin as a dynamic probe of the RNAP II mechanism, we substantially support our earlier model and observations. We identify three conformational states of the RNAP II EC with different sensitivities to α -amanitin (A43a, A43b, and A43c) (Fig. 1). The kinetic state herein designated A43a was not detected previously because A43a merged with the state here designated A43b (compare Figs. 1 and 2). The A43c EC strongly resists α -amanitin inhibition (Figs. 1 and 2). We conclude that our previous designation of A43c as the posttrans-

located EC is correct and that the posttranslocated state is resistant to α -amanitin inactivation (Fig. 3).

The RNAP II Secondary Pore as an Allosteric Site Controlling Transcription—The secondary pore of multisubunit RNAPs appears to be a major allosteric site for the regulation of transcription elongation (23), pausing, arrest, RNA cleavage, and transcriptional restart. α -Amanitin penetrates the pore (4) to regulate translocation and to arrest elongation at or before the translocation step. Microcin J25 is an inhibitor of bacterial RNAPs (24–27) that bears functional and structural resemblance to α -amanitin (Fig. 4).² Like α -amanitin, Microcin J25 penetrates the secondary pore of its cognate RNAP to inhibit initiation and elongation. Both α -amanitin and Microcin J25 contain cyclic octapeptide structures. α -Amanitin has a 6-hydroxy-Trp⁴–Cys⁸ covalent cross-bridge. The C-terminal

² J. Mukhopadhyay, E. Sineva, and R. Ebright, personal communication.

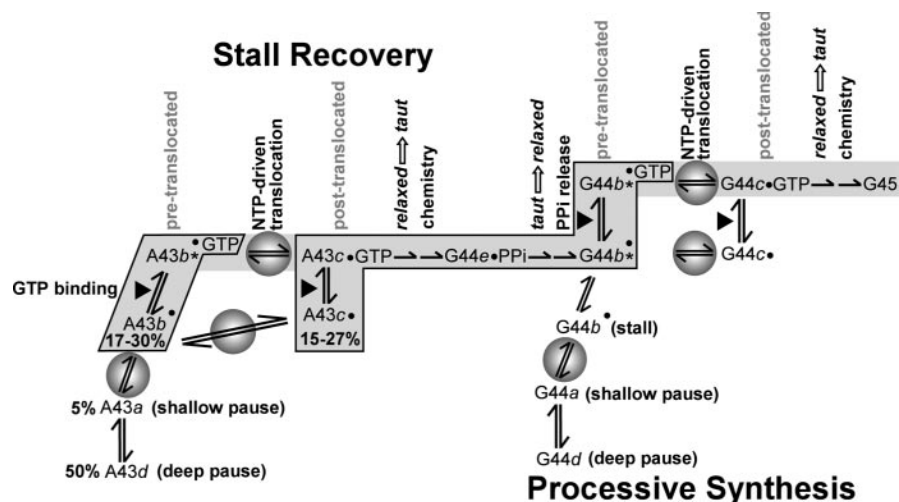


FIG. 3. **A model for α -amanitin inhibition of the RNAP II EC.** A43a and A43b reaction phases are highly susceptible to α -amanitin inhibition. A43c is strongly resistant. A43a and A43b are thought to be pretranslocated ECs. A43c is thought to be posttranslocated. Percent occupancy of A43a, A43b, and A43c states is estimated in Figs. 1 and 2 and in previous work (7). Variation in these estimates probably reflects further complexity in the RNAP II mechanism. *Gray shading* indicates the primary pathways for RNAP II elongation. Pathways for elongation in the presence of 1 mM α -amanitin are *outlined*. *Gray circles* indicate steps blocked by α -amanitin. *Black triangles*. *Bullets* indicate NTP binding sites oriented toward the main RNAP II channel (pretranslocated ECs) or the secondary pore (posttranslocated ECs) (7). *Lowercase italic letters* indicate different conformational states of the EC. In the running start protocol, A43 \rightarrow G44 represents recovery from the 60-s stall at A43, and G44 \rightarrow G45 represents normal processive synthesis, which is almost completely blocked by α -amanitin.

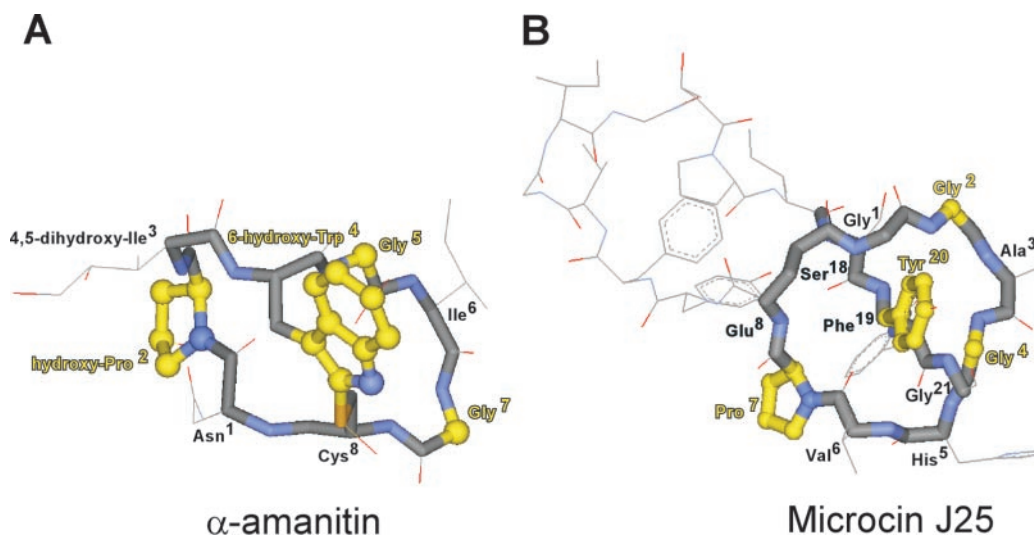


FIG. 4. **α -Amanitin and Microcin J25 are structurally related and functionally analogous peptides that penetrate the secondary pore of their cognate RNAPs to arrest transcription.** A, α -amanitin. B, Microcin J25. Similar features include the octapeptide rings and cross-bridges, each of which projects an aromatic amino acid. *Yellow-shaded residues* are similar in the two structures. Octapeptide rings and cross-bridges are indicated with *dark shading*. *Blue* indicates nitrogen. *Red* indicates oxygen. *Gray* or *yellow* indicates carbon. *Orange* indicates sulfur.

peptide tail of Microcin J25 (21 amino acids) forms a lariat protoknot through an N-terminal octapeptide covalent ring (Gly¹–Glu⁸) in imitation of the α -amanitin 6-hydroxy-Trp⁴–Cys⁸ cross-bridge. α -Amanitin residues hydroxy-Pro², -Gly⁵, and -Gly⁷ and 6-hydroxy-Trp⁴ appear to correspond to Microcin J25 Pro⁷, Gly², Gly⁴, and Tyr²⁰. Other peptides that penetrate the RNAP pore include the eukaryotic RNA cleavage and restart factors TFIIS/SII (28) and the analogous prokaryotic Gre factors (29, 30). TFIIS/SII was recently shown to be an allosteric effector of RNAP II pausing, separate from its role in RNA cleavage and transcriptional restart (15). A newly discovered class of bacterial antibiotics, the CBR703 series, also penetrates the secondary pore of bacterial RNAP and displays allosteric inhibitory effects on transcription (23).

Acknowledgments—We thank Y. Yamaguchi for the HDAg clone. We gratefully acknowledge R. Ebright for sharing information prior to publication.

REFERENCES

1. Wieland, T. (1968) *Science* **159**, 946–952
2. Wieland, T., Gotzendorfer, C., Zanotti, G., and Vaisius, A. C. (1981) *Eur. J. Biochem.* **117**, 161–164
3. Lindell, T. J., Weinberg, F., Morris, P. W., Roeder, R. G., and Rutter, W. J. (1970) *Science* **170**, 447–449
4. Bushnell, D. A., Cramer, P., and Kornberg, R. D. (2002) *Proc. Natl. Acad. Sci. U. S. A.* **99**, 1218–1222
5. Cramer, P., Bushnell, D. A., and Kornberg, R. D. (2001) *Science* **292**, 1863–1876
6. Gnat, A. L., Cramer, P., Fu, J., Bushnell, D. A., and Kornberg, R. D. (2001) *Science* **292**, 1876–1882
7. Nedialkov, Y. A., Gong, X. Q., Hovde, S. L., Yamaguchi, Y., Handa, H., Geiger, J. H., Yan, H., and Burton, Z. F. (2003) *J. Biol. Chem.* **278**, 18303–18312
8. Vassilyev, D. G., Sekine, S., Laptchenko, O., Lee, J., Vassilyeva, M. N., Borukhov, S., and Yokoyama, S. (2002) *Nature* **417**, 712–719
9. Holmes, S. F., and Erie, D. A. (2003) *J. Biol. Chem.* **278**, 35597–35608
10. Chafin, D. R., Guo, H., and Price, D. H. (1995) *J. Biol. Chem.* **270**, 19114–19119
11. Rudd, M. D., and Luse, D. S. (1996) *J. Biol. Chem.* **271**, 21549–21558
12. Palangat, M., and Landick, R. (2001) *J. Mol. Biol.* **311**, 265–282
13. Nudler, E. (1999) *J. Mol. Biol.* **288**, 1–12
14. Erie, D. A. (2002) *Biochim. Biophys. Acta* **1577**, 224–239

15. Zhang, C., Yan, H., and Burton, Z. F. (2003) *J. Biol. Chem.* **278**, 50101–50111
16. Lai, M. M. (1995) *Annu. Rev. Biochem.* **64**, 259–286
17. Taylor, J. M. (2003) *Trends Microbiol.* **11**, 185–190
18. Yamaguchi, Y., Filipovska, J., Yano, K., Furuya, A., Inukai, N., Narita, T., Wada, T., Sugimoto, S., Konarska, M. M., and Handa, H. (2001) *Science* **293**, 124–127
19. Funk, J. D., Nedialkov, Y. A., Xu, D., and Burton, Z. F. (2002) *J. Biol. Chem.* **277**, 46998–47003
20. Shapiro, D. J., Sharp, P. A., Wahli, W. W., and Keller, M. J. (1988) *DNA (N. Y.)* **7**, 47–55
21. Nedialkov, Y. A., Gong, X. Q., Yamaguchi, Y., Handa, H., and Burton, Z. F. (2003) *Methods Enzymol.* **371**, 252–262
22. Cochet-Meilhac, M., and Chambon, P. (1974) *Biochim. Biophys. Acta* **353**, 160–184
23. Artsimovitch, I., Chu, C., Lynch, A. S., and Landick, R. (2003) *Science* **302**, 650–654
24. Wilson, K. A., Kalkum, M., Ottesen, J., Yuzenkova, J., Chait, B. T., Landick, R., Muir, T., Severinov, K., and Darst, S. A. (2003) *J. Am. Chem. Soc.* **125**, 12475–12483
25. Rosengren, K. J., Clark, R. J., Daly, N. L., Goransson, U., Jones, A., and Craik, D. J. (2003) *J. Am. Chem. Soc.* **125**, 12464–12474
26. Bayro, M. J., Mukhopadhyay, J., Swapna, G. V., Huang, J. Y., Ma, L. C., Sineva, E., Dawson, P. E., Montelione, G. T., and Ebright, R. H. (2003) *J. Am. Chem. Soc.* **125**, 12382–12383
27. Yuzenkova, J., Delgado, M., Nechaev, S., Savalia, D., Epshtein, V., Artsimovitch, I., Mooney, R. A., Landick, R., Farias, R. N., Salomon, R., and Severinov, K. (2002) *J. Biol. Chem.* **277**, 50867–50875
28. Kettenberger, H., Armache, K. J., and Cramer, P. (2003) *Cell* **114**, 347–357
29. Sosunova, E., Sosunov, V., Kozlov, M., Nikiforov, V., Goldfarb, A., and Mustaev, A. (2003) *Proc. Natl. Acad. Sci. U. S. A.* **100**, 15469–15474
30. Laptenko, O., Lee, J., Lomakin, I., and Borukhov, S. (2003) *EMBO J.* **22**, 6322–6334